Canadian Journal of Remote Sensing
Journal canadien de télédétection

Crop Fraction Estimation from CASI Hyperspectral Data Using Linear Spectral Unmixing and Vegetation Indices

Journal:	*Canadian Journal of Remote Sensing*
Manuscript ID:	CJRS-05-0034.R3
Manuscript Type:	Review Paper
Date Submitted by the Author:	23-Feb-2006
Complete List of Authors:	Liu, Jiangui Miller, John Pattey, Elizabeth
Keyword:	hyperspectral, precision agriculture, Crop fraction, linear spectral unmixing, vegetation index, CASI

Research Paper

Crop Fraction Estimation from *casi* Hyperspectral Data Using Linear Spectral Unmixing and Vegetation Indices

Jiangui Liu[1,4], John R. Miller[2], Driss Haboudane[3], Elizabeth Pattey[4] and Klaus Hochheim[5]

[1]Earth Observations Laboratory, York University, 4700 Keele St., Toronto, Ontario M3J 1P3, Canada.
E-mail: liu_jiangui@yahoo.com. Fax: 1(613)-759-1515.

[2]Department of Earth and Space Science and Engineering, York University, Toronto, ON, M3J 1P3, Canada.

[3]Département des Sciences Humaines, UQAC, 555 boulevard de l'Université, Chicoutimi, QC, G7H 2B1, Canada.

[4]Agriculture and Agri-Food Canada, Central Experimental Farm, 960 Carling Ave., Ottawa, Ontario, K1A 0C6, Canada.

[5]Noetix Research Inc., 403-265 Carling Ave., Ottawa, Ontario, K1S 2E1, Canada.

Submitted to Canadian Journal of Remote Sensing

ABSTRACT

It is important to estimate vegetation fraction for regional weather forecasts, and in precision agriculture for assessing crop performance during emergence and early growth phases. In this study, two approaches, linear spectral unmixing and vegetation indices, were reviewed and evaluated for the estimation of crop fraction from hyperspectral data. Compact Airborne Spectrographic Imager (*casi*) hyperspectral data were acquired three times in the 2001 growing season over four agricultural fields to monitor crop growth conditions and develop procedures for delineating major sub-units for crop management. Crops planted in these fields included corn, soybean and wheat. Endmember spectra were extracted from *casi* data and used for linear spectral unmixing. Various vegetation indices, including Normalized Difference Vegetation Index (NDVI), Soil Adjusted Vegetation Index (SAVI), Optimized Soil-Adjusted Vegetation Index (OSAVI), Modified Soil Adjusted Vegetation Index (MSAVI) and Transformed Soil Adjusted Vegetation Index (TSAVI), as well as the recently developed indices Modified Triangular Vegetation Index (MTVI2), and the VI_{700} and VI_{green} indices, were evaluated with *casi* data and with simulated spectra using coupled PROSPECT and SAILH models. All these indices were highly correlated with measured crop fractions. A comparison study based on simulated spectra showed that MTVI2 maintained adequate sensitivity up to a higher crop coverage. A high coefficient of determination ($R^2 = 0.90$) and a low root mean square error (RMSE = 0.10) were obtained between measured and estimated crop fraction using MTVI2. The crop fraction derived from linear spectral unmixing was also highly correlated with the measured crop fraction ($R^2 = 0.94$ and RMSE = 0.08). However, determining endmember spectra in the linear spectral unmixing method remains a challenge. Using vegetation indices is a convenient method for crop fraction estimation with satisfactory accuracy.

Key Words:

Crop fraction, linear spectral unmixing, vegetation index, precision agriculture, *casi*, hyperspectral

INTRODUCTION

Vegetation fraction (VF) is defined as the fractional ground area occupied by the vertical projection of the crown or shoot area of vegetation. VF is necessary for modeling of water and energy fluxes at the surface (Roujean *et al*., 1997), and is a key parameter for the boundary layer parameterization in many land surface schemes (Deardorff, 1978). The fraction of the available solar radiation intercepted by foliage is one of the most important variables in crop growth monitoring, which, when associated with the energy use efficiency, can be used to predict crop productivity (Gitelson *et al*., 2002a, b). Crop fraction can be used as a surrogate for light interception, since there is a strong correlation between crop fraction and fraction of the incident solar radiation intercepted by foliage (Steven *et al*., 1986). Therefore, estimation of crop fraction is very important for monitoring crop growth.

The approaches for estimating VF from remote sensing data can be classified into four types. The first is the spectral mixture modeling (Ray and Murray, 1996; Roberts *et al*., 1993; Borel and Gerstl, 1994) which is based on the assumption that the measured pixel spectrum is either a linear or nonlinear combination of the component spectra within the sensor's instantaneous field-of-view; thus, fractions of components can be derived through spectral unmixing. The second type of approach relates VF with vegetation indices (Baret *et al*., 1995; Carlson and Ripley, 1997; Eastwood *et al*., 1997; Gitelson *et al*., 2002b). Generally speaking, most vegetation indices combine the reflectance of red and near-infrared bands, because the reflectance in these two regions provides a high contrast between vegetation and soil optical properties (Richardson and Wiegand, 1977). Two new indices, VI_{green} and VI_{700}, developed recently by Gitelson et al. (2002b), use the visible portions of the spectrum only. The reflectance of the red band is combined with the reflectance of the green band and the reflectance at 700 nm for VI_{green} and VI_{700}, respectively. The third approach is based on canopy reflectance models, or more specifically, a bi-directional reflectance model (Roujean *et al*., 1997; Peddle *et al*., 1999) to estimate VF from bi-directional reflectance simulations, in which the ground is considered to be composed of soil and dense vegetation. When both the sun and the sensor are at zenith, VF is equivalent to the fraction of solar radiation intercepted by the vegetation (Roujean *et al*., 1997). Since the solar zenith angle for data acquisition is rarely zero, bi-directional

reflectance models have to be inverted using a range of measurements with different view and solar angles in order to obtain VF. A fourth approach is based on the use of neural networks (NN) (Baret *et al*., 1995). This approach implicitly incorporates radiative transfer theory modeling for plant canopies in the interpretation of remote sensing data. Neural networks exploit the network training step to overcome the requirement to define many model and observational variables, and the difficulty associated with vegetation type dependencies.

It was acknowledged that nonlinear spectral unmixing (Borel *et al*., 1994; Johnson *et al*., 1992; Hapke, 1981) may be preferable to describe the resultant mixture spectrum of certain endmember distributions, and to make the vegetation cover more detectible (Guilfoyle *et al*., 2001; Ray and Murray, 1996). However, it makes the accurate quantitative assessment of vegetation fraction more difficult (Ray and Murray, 1996). Many studies demonstrate the ability of linear spectral unmixing to access relevant vegetation information (Lelong *et al*., 1998; Roberts *et al*., 1993). The deviation from the linear models can be attributed to the interaction of light with multiple components, which is useful for extracting other plant information (Ray and Murray, 1996; Roberts *et al*., 1993). For approaches based on vegetation indices, considerable efforts have been made to reduce external effects, mainly those due to the atmosphere and soil (Huete, 1988; Kaufman and Tanre, 1992).

In this study, the approaches based on linear spectral unmixing and vegetation indices are evaluated. The evaluated vegetation indices included NDVI, soil adjusted indices, as well as the newly developed MTVI2 (Haboudane *et al*., 2004), VI_{green} and VI_{700} (Gitelson *et al*., 2002b). The methods and capability of the two approaches for crop fraction estimation were studied and compared using Compact Airborne Spectrographic Imager (*casi*) hyperspectral data. The vegetation indices were also evaluated based on simulated spectra.

MATERIALS

The Study Site

The study site is located at the former Greenbelt Farm of Agriculture and Agri-Food Canada, Ottawa (45°18'N, 75°45'W). The four studied fields, named as F13, F16,

F23 and F25, are characterized by drained clay loam soil. In the 2001 growing season, F13, F16, F23 and F25 were planted with corn, soybean, corn and wheat, respectively. Specific Nitrogen (N) rates were applied within F25, as shown in Figure 1. No nitrogen was applied to the region marked with "0N". Regions marked with "41N" and "68N" received 41–kg N ha^{-1} and a recommended rate of 68-kg N ha^{-1}, respectively. Previous knowledge about the field management, soil and crop variability helped in selecting ground truth sites of contrasting biomass variability. Two, three, four and seven ground truth sites were deployed in these fields, respectively. Three intensive field campaigns (IFC) took place during this year, which coincided with the early vegetative (IFC1), active growth (IFC2) and reproductive (IFC3) development stages of wheat. In-situ measurements of crop features included fresh and dry biomass, leaf area index (LAI), leaf chlorophyll content, crop height, and crop fraction.

(Insert Figure 1 around here)

Measurement of Crop Fraction

As part of the overall ground survey plan, digital photos were taken at each ground truth site to collect information on crop fraction. The photos were taken from above the canopy at nadir to cover a ground area of about one square meter. The photos were classified using an unsupervised K-Means classifier implemented in PCI Geomatica (PCI Geomatica, 2001) to derive crop fraction.

Each photo was classified into 6 classes that represented vegetation, shaded vegetation, stubble, shaded stubble, soil, and shaded soil. The cover fraction of each class was determined from the classified photo. The crop fraction was calculated as the sum of the vegetation and shaded vegetation fractions. Stubble and soil fractions were calculated in the same way. Average fractions of stubble were low in the four fields, with 0.3%, 0.5%, 1.7% and 1.1% in fields F13, F16, F23 and F25, respectively.

The *casi* Hyperspectral Data

Hyperspectral images were acquired with the *casi* by the Center for Research in Earth and Space Technology (CRESTech). At each of the three IFCs (on June 13, June 26 and July 19, 2001), *casi* images were acquired in the multispectral and hyperspectral modes. For the hyperspectral mode, 72 contiguous spectral bands were acquired

which covered the visible and near-infrared portions of the solar spectrum with 7.5-nm bandwidth and 2-m spatial resolution.

The *casi* data were pre-processed to absolute ground reflectance by an operational procedure implemented in the Earth Observations Laboratory at York University. First, digital data collected by the *casi* sensor were converted to at-sensor radiance using the calibration coefficients determined in the laboratory. The CAM5S atmospheric correction model (O'Neill *et al*., 1997) was then used to transform the at sensor radiance to surface reflectance. Aerosol optical depth at 550 nm estimated from ground sunphotometer measurements, and the recorded illumination and view geometry were used in this step. In the third step, the aircraft motion effects were removed and the image was geo-referenced using the recorded navigation data. A flat field adjustment was then performed to compensate for residual errors in the water and oxygen absorption regions due to atmospheric correction. This was accomplished by inspecting the bands located in these absorption regions, and adjusting those bands with a detectible residual effect. Spectrally flat targets (road, roofs, etc.) found in the imagery were used to identify the bands that require adjustment, and to calculate the adjustment factors to remove the residual effects. In the last step, ground DGPS measurements were used for precise geometric correction and geo-referencing. The accuracy for the ground control points was within one pixel.

Data Simulation Using the PROSPECT and SAIL Models

Integration of leaf and canopy reflectance models has become a useful tool for remote sensing of vegetation studies (e.g., Jacquemoud *et al*., 1995; Zarco-Tejada *et al*., 2001). At both leaf and canopy levels, reflectance models have been adapted to provide the best tool for comparison studies (Jacquemoud *et al*., 2000). The PROSPECT leaf model (Jacquemoud and Baret, 1990) and the SAIL canopy model (Verhoef, 1984) were used to simulate crop canopy reflectance spectra. Simulated spectra were used in this study to assist the evaluation of vegetation indices. Input parameters to the PROSPECT model include leaf equivalent water content (Cw, g cm^{-2}), dry biomass content (Cm, g cm^{-2}), chlorophyll a+b content (Cab, μg cm^{-2}) and internal structure parameter (N_L). Cw was given a nominal value of 0.005. Cab was set to 45-μg cm^{-2}, an average value of field measurements of leaf chlorophyll content. According to Jacquemoud *et al*. (2000), 1.55 and 0.0045 g cm^{-2} were assigned to

parameters N_L and Cm, respectively. For the SAIL model, input parameters include: soil reflectance (Rs), leaf area index (LAI), leaf angle distribution (LAD), solar zenith angle (θs), view zenith angle (θv), and relative azimuth angle between view and sun direction (φ). LAI was given a range of values starting from 0 to a large value to represent crop fraction ranging from 0 to 1. The soil reflectance was extracted from a *casi* spectrum representing an average brightness soil in the fields. The complete set of model input parameters and variables are listed in Table 1.

Insert Table 1 around here.

METHODS

Defining the Endmembers

The classification of the digital photos from the sample sites of all four fields showed that the fractional cover of stubble was not significant in the 2001 growing season; therefore, stubble was not treated as an endmember. Shadow was introduced as an endmember to account for the shadowing effects (Smith *et al*. 1990; Sabol *et al*., 1992; Roberts *et al*., 1993; Lelong *et al*., 1998). Consequently, for each crop field, the following endmembers were determined: soil, shadow and crop.

Determination of Endmember Spectra

Determination of endmember spectra is crucial for spectral unmixing. Endmember spectra can be obtained from a spectral library (reference endmembers) or extracted from the image data (image endmembers) themselves. Because it is difficult to construct a spectral library that contains spectra accounting for all processes and factors influencing the image spectra, such as vegetation type, biological processes, background effects and radiation calibration (Bateson and Curtiss, 1996), extensive research efforts have focused on methods for extracting endmembers automatically, interactively or manually from images. A convex geometry method has been used for automatic extraction of the purest pixels from image data (Boardman 1993; Boardman and Kruse, 1994; Boardman *et al*., 1995; Lelong *et al*., 1998). It requires that pure pixels of each component exist in the image scene, and the fraction of each component has a wide distribution range. In case pure pixels do not exist, a two-step procedure was developed (Smith *et al*., 1990; Roberts *et al*., 1997). First, the image

endmembers are extracted automatically. Since these endmembers are usually mixtures of meaningful scene components, the second step is to search for the relevant reference endmembers within a spectral library. Bateson and Curtis (1996) developed a manual endmember selection scheme that operates on data clouds in parallel coordination presentation. It requires human interactions to derive the best individual endmembers. Tompkins *et al*. (1997) developed another approach for spectral mixture analysis, in which both the endmember spectra and the fractions of the endmembers were treated as unknowns. The practical application of this model uses any available *a priori* knowledge to reduce the number of equations. These various approaches demonstrate that there is no standard way for endmember extraction. Estimating endmember spectra from image data where pure pixels do not exist should rely on *a priori* knowledge about the scene.

In this study, crop fraction increased steadily from IFC1 to IFC3. Corn and soybean were at their early development stages at IFC1, with very low fraction coverage, and reached full coverage at IFC3. In the productive areas of Field F25, the crop fraction was high at IFC1 and reached full coverage at IFC2, whereas in the less productive areas, full coverage was reached at IFC3. In order to analyze the image data to extract endmember spectra, a principal component transformation was applied to the image data of each IFC. The first two principal components (PC) accounted for the majority of variability in the data (81.8% and 17.1% for IFC1, 74.9% and 22.7% for IFC2, 59.1% and 40.0% for IFC3); accordingly, data distributed in the space constructed by these two principal components (PC space) were inspected to identify the endmembers. Figure 2 shows the data distribution in the PC space, with the first and the second PCs plotted as the horizontal and vertical axes, respectively. The arrows show where soil and the three crops were located. Pixels from the three crop fields were distributed closely at IFC1, with significant overlap between corn and soybean, whereas at IFC2 and IFC3, they tended to be distributed separately.

(Insert Figure 2 around here)

In F25W, a field directly to the west of F25 (Figure 1), there were patches of bare soil between crop trial plots. All the pixels in the soil clusters in Figure 2 were from this field. Pure pixels of soil resided to the outer boundary of the data clouds, forming a distribution line opposite to the clusters of crops. The spreading of pure soil pixels

along the distribution line was mainly due to the different brightness. A medium brightness soil identified at the middle portion of the distribution line was used as endmember of soil, and was marked as "SL" in Figures 2a, b and c for the three IFCs. The assumption was that, spectral variability of soil in these fields was mainly due to soil brightness, and the soil brightness in F25W was in a same range as those of the other crop fields.

The endmembers of corn and soybean were identified from the PC space of IFC3, and were marked as "C" and "Soy" in Figure 2c. The respective image spectra were extracted from *casi* data of IFC3, and applied to the three IFCs. In Field F25, wheat reached full coverage at IFC2, so the endmember was identified directly in the PC space, and was marked as W2 in Figure 2b. However, since wheat was at the booting stage at IFC2, the canopy reflectance experienced a decrease in the near-infrared band. Accordingly, W2 was used for IFC2 only. There was no pure pixel of wheat at IFC1, but the high crop fraction in parts of the field showed a clear distribution trend that can be exploited to derive the location of endmember in the PC space (Figure 2a). Two curves bounding the data clouds of the wheat can be drawn, and extended to an intersection W1, which was considered a purest endmember for the wheat. The spectrum of W1 was then derived by inverse principal component transformation. At IFC3, wheat reached full coverage in F25. The significant variability in spectral signature was mainly due to the difference in the fraction of heads, green and dry leaves influenced by the variability of soil conditions. To account for this significant variability, two image endmembers, W31 and W32, were identified directly from the data clouds in the PC space (Figure 2c).

Pure pixels of shadow cannot be found in the crop fields. Lelong *et al*. (1998) used a constant value for shadow reflectance. In this study, the reflectance of shadow was assumed to be a constant of 0.02, which was close to the reflectance of tree shadow detected in the image. The principal component transformation was applied to this preset shadow spectrum, and its locations in the relative PC space were marked as "Sh" in Figures 2a, b and c.

Deriving Crop Fraction Using Linear Spectral Unmixing

The general equation and constraint that govern the linear spectral unmixing procedure are as follows (Sabol *et al*., 1992):

$$R_b = \sum_i f_i r_{ib} + \varepsilon_b \quad (1)$$

and

$$\sum f_i = 1, f_i \in [0,1] \quad (2)$$

where R_b is the pixel reflectance in band b, f_i is the area fraction of endmember i, r_{ib} is the reflectance of component i in band b, ε_b is the residual error of the model in band b. The residual error can also be calculated for each pixel over all bands.

The constrained linear spectral unmixing procedure was applied to the image data of the three IFCs, using the derived image endmember spectra. Shadow is not considered as a field descriptor, since its fraction (f_{shadow}) varies with sun zenith and azimuth angles. Therefore it was apportioned to crop and soil after unmixing. This was accomplished with an approximation that normalized the fractions of soil and crop by dividing their fractions by ($1-f_{shadow}$) (Adams *et al.*, 1995; Lelong *et al.*, 1998). Bateson and Curtiss (1996) pointed out that the fractions are relative abundances that need to be calibrated to ground measurements no matter how the endmembers are selected. This is possibly because the derived endmembers are not pure, or the mixing model is not accurate. In this study, the normalized fractions were taken directly as crop fraction without further calibration to the ground measurements.

Vegetation Indices Used in This Study

The well-known vegetation index NDVI (Rouse *et al.*, 1974) has been proven to be very robust and is correlated with various vegetation descriptors. Other indices have been developed to suppress soil background effects. The soil adjusted vegetation index (SAVI) is expressed as follows (Huete, 1988):

$$SAVI = (1+L)(R_{NIR}-R_{red})/(R_{NIR}+R_{red}+L) \quad (3)$$

where R_{NIR} and R_{red} are the near-infrared and red reflectance, respectively, and L is an adjusting factor that accounts for soil effects. The choice of a value for L is critical for soil effect minimization. A smaller adjusting factor is required for denser vegetation

than for sparser vegetation. Therefore, its selection requires the knowledge of vegetation density. A value of 0.5 was proposed to account for the first order soil variations for most conditions (Huete, 1988). Rondeaux *et al*. (1996) proposed the optimized SAVI (OSAVI) with an adjusting factor of 0.16 for agriculture studies. In order to account for different soil backgrounds, Qi *et al*. (1994) developed a modified SAVI (MSAVI). This index introduces a self-adjusting factor, rather than using a fixed value. In the estimation of LAI and APAR, Baret *et al*. (1989) proposed a transformed SAVI (TSAVI), which takes into account the soil brightness using soil line slope and intercept. Haboudane *et al*. (2004) proposed an index MTVI2 for the estimation of green LAI. With MTVI2, the variability of leaf chlorophyll content was suppresses while an adequate sensitivity was retained over a wide range of LAI. All these indices are based on the contrast between the red and near-infrared reflectance. However, Pickup *et al*. (1993) observed that in the data space constructed using the commonly used Landsat MSS bands 5 and 7, the separation between soil, rock and vegetated surface (both dry and green) is not as good as in the data space constructed using bands 4 and 5. Therefore they developed a cover index PD54 that uses MSS bands 4 and 5 for vegetation change detection (Pickup *et al*., 1993). Continuing this argument, Gitelson *et al*. (2002b) pointed out that in crops, the near infrared reflectance levels off or even decreases with the increase of vegetation cover due to the change in leaf angle or the loss of leaf chlorophyll content at the later development stages. Thus, they developed two indices, VI_{700}, which combines the reflectance at 700 nm and the red band, and VI_{green}, which combines reflectance at the green and the red bands, in the same manner as NDVI combines reflectance at near-infrared and red bands. These two indices were expected to be better estimators for green, as well as dry or senescent vegetation (Gitelson *et al*., 2002b).

Based on this review, vegetation indices NDVI, SAVI, OSAVI, MSAVI, TSAVI, MTVI2, VI_{green} and VI_{700} were included in this study. The formulae for these indices are listed in Table 2. Reflectance values of bands nearest to 800, 670, 550 and 700 nm were assigned to R_{NIR}, R_{red}, R_{green} and R_{700}, respectively. The wavelengths for these channels were 801.5, 672.4, 552.3 and 702.6 nm.

(Insert Table 2 around here)

Estimation of Crop Fraction from Vegetation Indices

In relating vegetation indices with vegetation fraction, Eastwood *et al*. (1997) used a linear regression model, whereas Purevdorj *et al*. (1998) used a second order polynomial regression model. Both vegetation fraction VF (Nilson, 1971; Baret *et al*., 1995) and vegetation indices VI (Clevers, 1989; Baret and Guyot, 1991; Richardson *et al*., 1992) can be expressed as an exponential function of LAI:

$$VF = 1 - \exp(-K_p LAI) \tag{4}$$

and

$$VI = VI_\infty + (VI_s - VI_\infty)\exp(-K_{VI} LAI) \tag{5}$$

where K_p is the canopy extinction coefficient dependent on canopy structure, and K_{VI} depends mainly on canopy architecture, sun and view directions, and leaf optical properties. VI_s and VI_∞ are the values of the vegetation index at LAI=0 and LAI=∞, respectively. Based on Equations (4) and (5), a semi-empirical model was developed to relate vegetation fraction with vegetation indices (Baret *et al*., 1995):

$$VF = 1 - [(VI - VI_\infty)/(VI_s - VI_\infty)]^{K_p/K_{VI}} \tag{6}$$

The semi-empirical model was used in this study for the indices based on near-infrared and red bands. Compared to the empirical models, it has a uniform formulation that enables a comparison between different indices, and all the three parameters, VI_s, VI_∞ and K_p / K_{VI} have physical meanings, which could be retrieved from canopy models. VI_s was calculated using a soil spectrum with average brightness in the fields. VI_∞ was calculated from PROSPECT and SAILH simulated spectra, with a large input LAI value. Input parameters for these models are reported in Table 1. The ratio K_p / K_{VI} was estimated from the measured crop fraction by a regression procedure using the obtained parameters VI_s and VI_∞. After the determination of VI_s, VI_∞ and K_p / K_{VI}, Equation (6) was used to calculate the crop fraction.

As introduced later in the paper, the two visible indices do not follow the model described in Equation (5); in this case the crop fraction was related to VI_{green} or VI_{700} with a linear model:

$$VF = a \times VI + b \tag{7}$$

where VI refers to VI_{green} or VI_{700}, a is the slope and b the intercept of the regression line.

RESULTS AND DISCUSSION

Spectra of the Selected Endmembers

Spectra of the selected endmembers are shown in Figure 3. Shadow, corn and soybean were represented by a single spectrum for IFC1, IFC2 and IFC3, while wheat and soil were represented by different spectra at the three IFCs. The near-infrared reflectance of the wheat endmember changed from 0.57 at IFC1 to about 0.50 at IFC2, and at IFC3, it decreased further to 0.39 for W31 and 0.26 for W32. The red reflectance of W32 increased remarkably as a result of senescence.

(Insert Figure 3 around here)

Results from Linear Spectral Unmixing

The normalized crop fraction from the linear spectral unmixing procedure was highly linearly correlated with the measured crop fraction (R^2 = 0.94 and RMSE = 0.08). Figure 4a shows the comparison between measured and estimated crop fraction for corn, soybean and wheat at IFC1-2 and IFC3. Both endmembers of wheat at IFC3 represented full crop coverage. The fractions of these two endmembers were summed to give wheat coverage fraction. These samples converged close to full crop fraction (i.e., 1.0) for estimation and measurements, demonstrating that most of the variability in F25 can be modelled with these two image endmembers. Comparison between green LAI and the fractions of these two endmembers is shown in Figure 4b. It is clear that W32 represented wheat at a more senescent stage than W31. Here, "green LAI" refers to LAI of living leaves regardless of their photosynthetic capacity (Haboudane *et al*., 2004).

(Insert Figure 4a, b around here)

The field variability that cannot be modeled using the selected endmembers can be identified by the residual image (Gillespie *et al*., 1990). A higher value in the residual image indicates a larger deviation from the typical condition represented by the endmembers chosen. The residual images of F23, F25 and F16 were shown in Figure 5. F13 was not shown because it is less variable due to homogeneous soil conditions and uniform management. F16 was homogeneous in soil properties and uniform in management practice, the variability in the residual image was limited. In F23, variability in the residual images was mainly due to the variability of soil properties, which were not accounted for using the soil endmembers generated from F25W. In F25, the variability was due to both the variability in soil properties and the rates of nitrogen application, which caused significant variations in growing conditions and the spectral signatures. Region of 0N was barely detectable during IFC1, but became much more pronounced at IFC2 and IFC3. Although it was not as clear as in region 0N, the difference between 41N and 68N regions began to emerge at IFC2 and became more evident at IFC3. The residual images also outlined a region at the top part of Field F25. This region has a pronounced slope toward the creek between F23 and F25.

(Insert Figure 5 around here)

Soil Effects on Linear Spectral Unmixing

Pixel-based spectral unmixing in remote sensing is a highly uncertain process (Petrou and Foschi, 1999). The origin of the uncertainty comes partly from noise that was introduced to remote sensing data, partly from the intrinsic variability of the component materials. This uncertainty introduces spectral variability in the endmembers. When a single spectrum is used to represent an endmember, the resulting component fractions will be uncertain.

The soil distribution line in Figure 2 demonstrated the spectral variability of pure soil. Shadow (marked as “Sh”) resided approximately on the extension of this soil line. Along the distribution line toward shadow “Sh”, soil became darker. In this study, the spectrum of a medium brightness soil was used for unmixing. In the case of IFC1, this means although pixels of background soil can be anywhere between dark soil at “A” and bright soil at “B”, they were all assumed to be at “SL” (Figure 2a). This surely led to errors in crop fraction estimation. Since pixels of pure soil and shadow were

approximately on the same line, the major influence of using a single spectrum on different background soil would be a change in the relative fractions of soil and shadow, with minimal influence on crop fraction.

If the selected endmember of soil is brighter than the background soil, then the fraction of shadow (f_{shadow}) will be over-estimated by the linear spectral unmixing algorithm. Since crop fraction was normalized by dividing ($1-f_{shadow}$) to absorb the portion of shaded crop, it will be over-estimated as a result. Following the same reasoning, if the selected endmember of soil is darker than the background soil, the crop fraction will be under-estimated.

Figure 6 provides a simple evaluation of the impact of soil brightness on crop fraction estimation using linear spectral unmixing. The experiment was carried out in Field F25 at IFC1. Unmixing was applied twice using two different brightness soil as endmember, bright soil at "B" and dark soil at "A" (Figure 2a). The spectra of these two soils were shown in Figure 6a. Endmembers of wheat and shadow were the same as the spectra illustrated in Figure 3. Figure 6b shows the comparison of the estimations using these two soils as endmembers. It can be observed that crop fractions estimated using a brighter soil as endmember are higher than that estimated using a darker soil. The maximum difference was 5.3%. It can be concluded that, the crop fraction estimation error due to soil should be smaller than 5.3%.

(Insert Figure 6 around here)

Results from Vegetation Indices

The calculated VI_s, VI_∞ and K_p / K_{VI} for the indices based on the reflectance of near-infrared and red bands, and the slopes and intercepts of the linear regression lines for the two visible indices, are listed in Table 3. These parameters were used to calculate crop fractions from *casi* data using Equation (6) and (7). Correlation between measured and estimated crop fractions are summarised in Table 4. Figure 7 shows the comparison between measured and estimated crop fractions. The samples of closed wheat canopy at IFC3 were excluded from the statistics and the figure, since all the vegetation indices dropped drastically due to significant senescence.

(Insert Table 3 and 4 around here)

(Insert Figure 7 around here)

Satisfactory results were obtained from the two visible indices using linear regression model, and from the other indices using the semi-empirical model. Significant correlation was observed between the measured and the estimated crop fractions for all the evaluated vegetation indices. RMSE was 0.12 for VI_{700}, 0.11 for MSAVI and VI_{green}, and smaller than 0.11 for all the other indices. The R^2 ranged from 0.87 for VI_{700} to 0.93 for NDVI. TSAVI and OSAVI provided very similar estimation of crop fraction. The relationships between the estimated and measured crop fractions for the two visible indices, VI_{green} and VI_{700}, were different from the other indices, showing less sensitivity at higher LAI (Figure 7).

To get a better view of the vegetation indices tested in this study, the sensitivity of the indices to LAI was evaluated based on the simulated spectra using the PROSPECT and SAIL models. LAI was used for the evaluation because it was a parameter of the SAIL model, and could be related with crop fraction through Equation (4). Evaluation of the sensitivity to LAI should provide insight on the performance of the indices in crop fraction estimation. The sensitivity was calculated as $\Delta VI/[\Delta LAI(VI_\infty - VI_s)]$. The division by $(VI_\infty - VI_s)$ was to scale all the indices to the same range [0; 1]. Figure 8a shows the dependencies of the scaled indices to LAI, and Figure 8b shows the sensitivity of the scaled indices to LAI. For the evaluated indices based on near-infrared and red bands, the sensitivity to LAI can be approximated by an exponential equation. This is in conformity with Equation (5), from which the following equation can be derived:

$$dVI/[(VI_\infty - VI_s)dLAI] = K_{VI}\exp(-K_{VI}LAI) \quad (8)$$

The sensitivity at LAI = 0 was equivalent to K_{VI}. Indices with higher K_{VI} also had a higher decreasing rate of sensitivity with the increase of LAI. NDVI, OSAVI, TSAVI and SAVI had a higher sensitivity when LAI was low, and became relatively insensitive when LAI was high. MTVI2 and MSAVI had an adequate sensitivity at both high and low LAI. The sensitivity of the two visible indices, VI_{green} and VI_{700}, did not follow the relation given in Equation (8). Their sensitivity remained stable until LAI increased to about 1.5, and then decreased. This demonstrated that Equation (6) is not applicable to VI_{green} and VI_{700}.

(Insert Figure 8 around here)

Since MTVI2 maintained adequate sensitivity over a wide range of LAI (Figure 8b), and presented reduced sensitivity to soil effects and leaf chlorophyll variability (Haboudane *et al*., 2004), this index was chosen for estimating crop fraction. The equation is written as follows:

$$VF = 1 - \left[(MTVI2 - 0.918)/(0.001 - 0.918)\right]^{1.042} \quad (9)$$

Spatial Variability of Crop Fraction

Maps of crop fractions were generated using an index-based approach, from MTVI2, and using linear spectral unmixing in order to study the spatial variability and seasonal/temporal variations in the fields. Figure 9 shows the results from MTVI2 (upper) and linear spectral unmixing (lower) of fields F23 (Corn), F25 (Wheat) and F16 (Soybean) for the three IFCs. The maps corresponding to the relatively homogeneous Field F13 were not shown.

(Insert Figure 9 around here)

Soybean planted in F16 had a homogeneous development with very small spatial variability. The crop fraction for soybean increased from around 0.15 at IFC1, to about 0.65 at IFC2 and full coverage at IFC3. Corn in Field F23 showed significant spatial variability due to the differences in soil properties and topography. At IFC1, crop fraction of corn in most of the area was around 0.1, with small areas reaching 0.3. A wide range of crop fractions (i.e., 0.3-0.8) were observed at IFC2 and full coverage was reached at IFC3. Crop variability in F25 at IFC1 and IFC2 were mainly induced by the amount of nitrogen applied and by the soil properties, while at IFC3, they merely reflected the differences in the stage of senescence. The highest crop fraction (about 0.9) observed at IFC1 in the north-east corner of F25 is an area with a soil classified as sandy clay loam to fine sandy loam, which is favourable for crop development; it also received the recommended nitrogen application enabling early and uniform emergence. The crop development in the region of 0N was delayed, with coverage of only 0.4 at IFC1. At IFC1, the area with the lowest crop fraction (<0.3) detected at the upper part of F25 was characterized by very low organic matter content as a result of erosion due to the slope heading toward the creek flowing

between Fields F23 and F25. The diagonal strips (NW to SE) detected at IFC3 are filled old water channels that provided extra water, which made the crop senesce slower in this region.

Although there were discrepancies between the estimates from linear spectral unmixing and vegetation indices, both approaches revealed the spatial variability and temporal variation of crop fractions very well, except at IFC3. Through pixel-by-pixel comparison, correlation coefficients between crop fractions estimated from the two approaches for soybean, corn and wheat were 0.94, 0.92 and 0.97 at IFC1, 0.98, 0.99 and 0.97 at IFC2, and 0.76, 0.75 and 0.50 at IFC3, respectively. A reason for the decreased correlation at IFC3 was the reduced dynamic range of crop fractions.

CONCLUSIONS

Crop fractions of corn, soybean and wheat were estimated from multi-temporal *casi* hyperspectral image data using two approaches, linear spectral unmixing and vegetation indices. Three endmembers, crop, soil and shadow were used in the unmixing procedure. The effect of soil to the result using linear spectral unmixing was evaluated. The performance of vegetation indices NDVI, SAVI, OSAVI, TSAVI, MSAVI, MTVI2, and the newly developed visible indices VI_{green} and VI_{700} were evaluated using *casi* data and simulated spectra. The study showed that both approaches revealed the spatial variability and temporal variation of crop fraction well. The coefficients of determination between measured and estimated crop fraction using linear spectral unmixing and MTVI2 were higher than 0.9, with RMSE about 0.1 for MTVI2 and 0.08 for linear spectral unmixing.

Spectral unmixing is a useful tool that allows the exploration of the full information obtained by hyperspectral sensors. Extraction of endmember spectra from image data is crucial. Although it is the most laborious step, the endmembers extracted could account for the variability from other factors than crop fraction, such as canopy structure and growth condition. The crop fraction is determined in multidimensional space constructed by the endmembers. The resulting residual images reveal information that cannot be modelled by the extracted endmember spectra, which can be interpreted according to the variability of the endmembers, such as different background soil and crop growth conditions, etc. This is an asset that could be exploited further.

Compared with the spectral unmixing method, vegetation indices simply convert the spectral information into a single variable by combining the reflectance of a few spectral bands. Although this may cause information loss, the advantage rests in its simplicity. This study showed that all the evaluated indices could be used for crop fraction estimation with a satisfactory accuracy. Based on the experimental data sets, the indices had comparable estimation results.

Comparison of the sensitivity to LAI based on simulated spectra indicated that the relations between vegetation indices and crop fraction for the two visible indices, VI_{green} and VI_{700}, were not the same as the other indices. MTVI2 and MSAVI retained an adequate sensitivity at both low and high LAI.

Spectral uncertainty is a factor that affects the accuracy of both spectral unmixing and vegetation indices. Here the uncertainty refers to spectral variability that comes from factors other than crop fraction, such as the background soil and other crop growth conditions; therefore, interpretation of the obtained crop fraction should incorporate the information related to these aspects.

ACKNOWLEDGEMENTS

The authors are indebted to Lawrence Gray, Phil Brasher and Heidi Beck of Aviation International for efficiently executing *casi* airborne field campaigns, to Dave Dow, Mathew Hinther and Matt McKechnie for their fieldwork. The study was funded by the Government Related Initiatives Program (GRIP) project between the Canadian Space Agency and Agriculture and Agri-Food Canada, a CSA contract to Noetix (9F028-1-4011/13), and the GEOIDE Networked Centre of Excellence. AAFC contribution number: 05-523.

REFERENCES

Adams, J. B., Sabol, D. E., Kapos, V., Filho, R. A., Roberts, D. A., Smith, M. O. and Gillespie, A. R. 1995. Classification of multispectral images based on fractions of endmembers: Application to land-cover change in the Brazilian Amazon. *Remote Sensing of Environment.* Vol. 52, pp. 137-154.

Baret, F., Guyot, G. and Major, D. J. 1989. TSAVI: a vegetation index that minimizes soil brightness effects on LAI and APAR estimation. In: *Proceedings of 1989 International Geoscience and Remote Sensing Symposium and 12th Canadian Symposium on Remote Sensing*, Vancouver, Canada, pp. 1355-1358.

Baret. F. and Goyot, G. 1991. Potential and limits of vegetation indices for LAI and APAR assessment. *Remote Sensing of Environment.* Vol. 35, PP. 161-173.

Baret, F., Clevers, J. G. P. W. and Steven, M. D. 1995. The robustness of canopy gap fraction estimation from red and near-infrared reflectance: A comparison of approaches. *Remote Sensing of Environment.* Vol. 54, pp. 141-151.

Bateson, A. and Curtis, B. 1996. A method for manual endmember selection and spectral unmixing. *Remote Sensing of Environment.* Vol. 55, pp. 229-243.

Boardman, J. 1993. Automated spectral unmixing of AVIRIS data using convex geometry concepts. In: *Summary of the 4th Annual JPL Airborne Geoscience Workshop,* Washington, D.C., USA. JPL publication 93-26, Vol. 1, pp. 11-14.

Boardman J. W. and Kruse, F. A. 1994. Automated spectral analysis: A geologic example using AVIRIS data, north Grapevine Mountains, Nevada. In *Proceedings, Tenth Thematic Conference on Geologic Remote Sensing,* May 9-12, 1994, Environmental Research Institute of Michigan, San Antonio, TX, USA. pp. 407-418.

Boardman, J. W., Kruse, F. A. and Green, R. O. 1995. Mapping target signatures via partial unmixing of AVIRIS data. In: *Summaries of 5th Annual JPL Airborne Geoscience Workshop*, Pasadena, CA, USA. JPL Publication 95-1, Vol. 1, pp. 23-26.

Borel, C. C. and Gerstl, A. W. 1994. Nonlinear spectral mixing models for vegetation and soil surfaces. *Remote Sensing of Environment.* Vol. 47, pp. 403-416.

Carlson, T. N. and Ripley, D. A. 1997. On the relationship between NDVI, fractional vegetation cover, and leaf area index. *Remote Sensing of Environment.* Vol. 62, pp. 241-252.

Clevers, J. G. P. W. 1989. The application of a weighted infrared vegetation index for estimating leaf area index by correcting for soil moisture. *Remote Sensing of Environment.* Vol. 29, pp. 25-37.

Deardorff, J. W. 1978. Efficient prediction of ground surface temperature and moisture with inclusion of a layer of vegetation. *Journal of Geophysical Research.* Vol. 20, pp. 1889-1903.

Eastwood, J. A., Yates, M. G., Thomson, A. G. and Fuller, R. M. 1997. The reliability of vegetation indices for monitoring saltmarsh vegetation cover. *International Journal of Remote Sensing.* Vol. 18, No. 18, pp. 3901-3907.

Gillespie, A. R., Smith, M. O., Adams, J. B., Willis, S. C., Fischer, A. F., III. and Sabol, D. E. 1990. Interpretation of residue images: Spectral mixture analysis of AVIRIS images, Owens Valley, California, in *Proceedings of 2nd Airborne Visible/Infrared Imaging Spectrometer (AVIRIS) Workshop*, 4-5 June, 1990, Pasadena, CA, USA. Edited by R. O. Green. pp. 243-270.

Gitelson, A. A., Stark, R., Grits, U., Rundquist, D., Kaufman Y. and Derry, D. 2002a. Vegetation and soil lines in visible spectral space: a concept and technique for remote sensing of vegetation fraction. *International Journal of Remote Sensing*. Vol. 23, No. 13, pp. 2537-2562.

Gitelson, A. A., Kaufman Y. J., Stark, R. and Rundquist, D. 2002b. Novel algorithms for remote estimation of vegetation fraction. *Remote Sensing of Environment.* Vol. 80, pp. 76-87.

Guilfoyle, K. J., Althouse, M. L. and Chang, C. I. 2001. A quantitative and comparative analysis of linear and nonlinear spectral mixture models using radial

basis function neural networks. *IEEE Transaction on Geoscience and Remote Sensing.* Vol. 39, No. 8, pp. 2314-2318.

Haboudane, D., Miller, J. R., Pattey, E., Zarco-Tejada, P. J. and Strachan, I. B. 2004. Hyperspectral vegetation indices and novel algorithms for predicting green LAI of crop canopies: Modeling and validation in the context of precision agriculture. *Remote Sensing of Environment.* Vol. 90, pp. 337-352.

Hapke, B. 1981. Bidirectional reflectance spectroscopy, I: Theory. *Journal of Geophysical Research.* Vol. 86, pp. 3039-3054.

Huete, A. R. 1988. A soil-adjusted vegetation index (SAVI). *Remote Sensing of Environment.* Vol. 25, pp. 295-309.

Jacquemoud, S. and Baret,F. 1990. PROSPECT: A model of leaf optical properties spectra. *Remote Sensing of Environment.* Vol. 34, pp. 75-91.

Jacquemoud, S., Baret, F., Andrieu, B., Danson, F.M. and Jaggard, K. 1995. Extraction of vegetation biophysical parameters by inversion of the PROSPECT+SAIL models on sugar beet canopy reflectance data: Application to TM and AVIRIS sensors. *Remote Sensing of Environment.* Vol. 52, pp. 163-172.

Jacquemoud, S., Bacour, C., Poilve, H. and Frangi, J. –P. 2000. Comparison of four radiative transfer models to simulate plant canopies reflectance: Direct and inverse mode. *Remote Sensing of Environment.* Vol. 74, pp. 471-481.

Johnson, P. E., Smith, M. O. and Adams, J. B. 1992. Simple algorithms for remote determination of mineral abundances and particle sizes from reflectance spectra. *Journal of Geophysical Research.* Vol. 97(E2), pp. 2649-2657.

Kauffman, Y. J. and Tanre, D. 1992. Atmospherically resistant vegetation index (ARVI) for EOS-MODIS. *IEEE Transaction on Geoscience and Remote Sensing.* Vol. 30, No. 2, pp. 261-270.

Lelong, C. C. D., Pinet, P. C. and Poilve, H. 1998. Hyperspectral imaging and stress mapping in agriculture: A case study on wheat in Beauce (France). *Remote Sensing of Environment.* Vol. 66, pp. 179-191.

Nilson, T. 1971. A theoretical analysis of the frequency of gaps in plant stands. *Agricultural meteorology.* Vol. 8, pp. 25-38.

O'Neill, N.T., Zagolski, F., Bergeron, M., Royer, A., Miller, J. R. and Freemantle, J. 1997. Atmospheric correction validation of *casi* images acquired over the BOREAS southern study area. *Canadian Journal of Remote Sensing*. Vol. 23, pp. 142-162.

PCI Geomatica, 2001. EASI/PACE to Geomatica, Version 8.2.3.

Peddle, D. R., Hall, F. G. and LeDrew, E. F. 1999. Spectral mixture analysis and Geometric-Optical reflectance modeling of Boreal Forest Biophysical structure. *Remote Sensing of Environment.* Vol. 67, pp. 288-297.

Petrou, M. and Foschi P. G. 1999. Confidence in linear spectral unmixing of single pixels. *IEEE Transaction on Geoscience and Remote Sensing.* Vol. 37, No. 1, pp. 624-626.

Pickup, G., Chewings, V. H. and Nelson, D. J. 1993. Estimating changes of vegetation cover over time in arid rangelands using Landsat MSS data. *Remote Sensing of Environment.* Vol. 43, pp. 243-263.

Purevdorj, Ts., Tateishi, R., Ishiyam, T. and Honda, Y. 1998. Relationship between percent vegetation cover and vegetation indices. *International Journal of Remote Sensing.* Vol. 19, No. 28, pp. 3519-3535.

Qi, J., Chehbouni, A., Huete, A. R., Keer, Y. H. and Sorooshian, S. 1994. A modified soil vegetation adjusted index. *Remote Sensing of Environment.* Vol. 48, pp. 119-126.

Ray, T. W. and Murray, B. C. 1996. Nonlinear spectral mixing in desert vegetation. *Remote Sensing of Environment.* Vol. 55, pp. 59-64.

Richardson, A. J. and Wiegand, C. L. 1977. Distinguishing vegetation from soil background information. *ASPRS Photogrammetric Engineering and Remote Sensing.* Vol. 43, pp. 1541-1552.

Richardson, A. J., Wiegand, C. L., Wanjura, D. F., Dusek, D. and Steiner, J. L. 1992. Multi-site analysis of spectral-biophysical data for sorghum. *Remote Sensing of Environment.* Vol. 41, pp. 71-82.

Roberts, D. A., Smith, M. O., and Adams, J. B. 1993. Green vegetation, nonphotosynthetic vegetation, and soil in AVIRIS data. *Remote Sensing of Environment.* Vol. 44, pp. 255-269.

Roberts, D. A., Green, R. O. and Adams, J. B. 1997. Temporal and spatial patterns in vegetation and atmospheric properties from AVIRIS. *Remote Sensing of Environment.* Vol. 62, pp. 223-240.

Roujean, J.-L., Tanre, D., Breon, F.-M. and Deuze, J.-L. 1997. Retrieval of land surface parameters from airborne POLDER bi-directional reflectance distribution function during HAPEX-Sahel. *Journal of Geophysical Research.* Vol. 102, pp. 11201-11218.

Rondeaux, G., Steven, M. and Baret, F. 1996. Optimization of soil-adjusted vegetation indices. *Remote Sensing of Environment.* Vol. 55, pp. 95-107.

Rouse, J. W., Haas, R. H., Schell, J. A., Deering, D. W. and Harlan, J. C. 1974. Monitoring the vernal advancements and retrogradation of natural vegetation. *NASA/GSFC, Final Report*, Greenbelt, MD, USA, pp. 1-137.

Sabol, D. E., Adams, J. B. and Smith, M. O. 1992. Quantitative sub-pixel spectral detection of targets in multispectral images. *Journal of Geophysical Research.,* Vol. 97(E2), pp. 2659-2672.

Smith, M. O., Ustin, S. L., Adams, J. B. and Gillepsie, A. R. 1990. Vegetation in deserts: I. A regional measure of abundance from multi-spectral images. *Remote Sensing of Environment.* Vol. 31, pp. 1-26.

Steven, M. D., Biscoe, P. V., Jaggard, K. W. and Paruntu, J. 1986. Foliage cover and radiation interception. *Field Crops Research.* Vol. 13, pp. 75-87.

Tompkins, S., Mustard, J. F., Pieters, C. M. and Frosyth, D. W. 1997. Optimization of endmembers for spectral mixture analysis. *Remote Sensing of Environment.* Vol. 59, pp. 472-489.

Verhoef, W. 1984. Light scattering by leaf layers with applications to canopy reflectance modeling: The SAIL model. *Remote Sensing of Environment.* Vol. 16, pp. 125-141.

Zarco-Tejada, P. J., Miller, J. R., Noland, T. L., Mohammed, G. H. and Sampson, P. H. 2001. Scaling-up and model inversion methods with narrow-band optical indices

for chlorophyll content estimation in closed forest canopies with hyperspectral data. *IEEE Transaction on Geoscience and Remote Sensing*. Vol. 39, No. 7, pp.1491– 1507.

Table 1. Input parameters for the PROSPECT leaf model and SAILH canopy model.

Leaf model parameters				
Cw (g cm^{-2})	Cm (g cm^{-2})	N_L	Cab (μg cm^{-2})	
0.005	0.0045	1.55	45	
Canopy model parameters				
LAD	LAI	θs	θv	φ
Spherical	[0, 12]	30°	0°	0°
Soil reflectance used in the SAIL model				
Wavelength (nm)	550	670	700	800
Reflectance	0.15	0.20	0.21	0.26

Note: Cw, leaf equivalent water content; Cm, leaf dry biomass content; N_L, leaf internal structure parameter; Cab, leaf chlorophyll content including chlorophyll a and b; LAD: leaf angle distribution; LAI, leaf area index; θs, solar zenith angle; θv, sensor view angle; φ, relative azimuth angle between view and sun direction.

Table 2. Vegetation indices evaluated in this study.

Formulae	Reference
$NDVI = (R_{NIR} - R_{red})/(R_{NIR} + R_{red})$	Rouse *et al.*, 1974
$SAVI = 1.5 \times (R_{NIR} - R_{red})/(R_{NIR} + R_{red} + 0.5)$	Huete, 1988
$OSAVI = 1.16 \times (R_{NIR} - R_{red})/(R_{NIR} + R_{red} + 0.16)$	Rondeaux *et al*, 1996
$MSAVI = (2 \times R_{NIR} + 1 - \sqrt{(2 \times R_{NIR} + 1)^2 - 8 \times (R_{NIR} - R_{red})})/2$	Qi *et al.*, 1994
$MTVI2 = \dfrac{1.5 \times [1.2 \times (R_{800} - R_{550}) - 2.5 \times (R_{670} - R_{550})]}{\sqrt{(2 \times R_{800} + 1)^2 - (6 \times R_{800} - 5 \times \sqrt{R_{670}}) - 0.5}}$	Haboudane *et al.*, 2004
$TSAVI = \alpha \times (R_{NIR} - \alpha R_{red} - \beta)/(\alpha R_{NIR} + R_{red} - \alpha\beta + 0.08 \times (1 + \alpha^2))$	Baret *et al.*, 1989
$VI_{green} = (R_{green} - R_{red})/(R_{green} + R_{red})$	Gitelson *et al.*, 2002b
$VI_{700} = (R_{700} - R_{red})/(R_{700} + R_{red})$	Gitelson *et al.*, 2002b

Note: R is the reflectance, and its subscript refers to the spectral position in nm. NIR, red and green refer to near infrared, red and green bands. Soil line parameters α=1.2439 (slope) and β=0.0057 (intercept), were obtained from the soil scatter-plot from *casi* data sets in the same fields.

Table 3. Calculated parameters for estimating crop fraction from vegetation indices.

	NDVI	SAVI	OSAVI	TSAVI	MSAVI	MTVI2		VI_{700}	VI_{green}
VI_s	0.121	0.087	0.104	0.001	0.077	0.001	a	2.046	1.624
VI_∞	0.935	0.765	0.856	0.730	0.867	0.918	b	0.056	0.289
K_p/K_{VI}	0.710	1.023	0.857	0.818	1.174	1.042			

Note: left part, parameters for the semi-empirical model (Equation (6)); right part, parameter for the linear model (Equation (7)); VI_s, index value with LAI = 0; VI_∞,

index value with LAI = ∞; K_p / K_{VI}, a parameter dependent on canopy structure and sun and view angles; a and b, the slope and intercept of the regression line.

Table 4. Comparison between measured and estimated crop fraction using vegetation indices.

	NDVI	SAVI	OSAVI	TSAVI	MSAVI	MTVI2	VI_{700}	VI_{green}
R^2	0.93	0.90	0.92	0.92	0.90	0.90	0.87	0.89
RMSE	0.09	0.10	0.09	0.09	0.11	0.10	0.12	0.11
F	472	331	399	406	327	345	240	290

Note: R^2, the coefficient of determination; RMSE, root mean square error; F, the F-distribution value. Critical value of F is $F_{0.01,1,37}$<7.56; samples of wheat at IFC3 were not included in the statistics.

List of Figures

Figure 1. Location of the study site and the field boundaries. The sectors within the wheat field, F25, coincide to different nitrogen (N) application rates (68 N=68 kg N ha^{-1}; 41 N=41 kg N ha^{-1}; 0N=0 kg N ha^{-1}). F25W is the west section of field 25 in which bare soil presented throughout the season.

Figure 2. Data distribution in the principal component space for IFC1 (a), IFC2 (b) and IFC3 (c). The first and the second principal components are plotted as horizontal and vertical axes, respectively. Sh, Soy, C and SL in the figure denominate to the endmember of shadow, soybean, corn and soil; W1 and W2 denominate wheat endmembers at IFC1 and IFC2, W31 and W32 denominate the two endmembers of wheat, representing wheat at different senescent stages at IFC3; A and B represent dark and bright soil respectively, as detected in the data cloud of IFC1; The arrows point to where the cover types are mostly located in the data cloud.

Figure 3. Endmember spectra used in the linear spectral unmixing.

Figure 4. Results from linear spectral unmixing: (a) comparison between measured and estimated crop fraction, and (b) relationship between green LAI and the derived fractions of the two wheat endmembers at IFC3.

Figure 5. Residual images from linear spectral unmixing of Fields F23 (upper), F25 (middle) and F16 (lower) at IFC1 (a), IFC2 (b) and IFC3 (c). The values of the scale bars in the images were multiplied by 100.

Figure 6. Soil effects on linear spectral unmixing as evaluated for wheat at IFC1. a: spectra of dark and bright soil (A and B in Figure 2a); b: comparison between wheat fraction estimation with bright and dark soil.

Figure 7. Comparison between measured and estimated crop fraction using vegetation indices: samples from F25 (wheat) at IFC3 were not plotted.

Figure 8. Evaluation of the vegetation indices using the PROSPECT and SAILH models simulated data: (a) scaled vegetation indices, and (b) sensitivity of the scaled vegetation indices as a function of LAI. Here the sensitivity is the ratio between the variation of the scaled index to the variation of LAI.

Figure 9. Maps of crop fraction estimated from MTVI2 (upper) and linear spectral unmixing (lower) for corn in Field F23, wheat in Field F25 and soybean in Field F16. From left to right, the maps represent IFC1, IFC2 and IFC3, respectively.

Figure 1

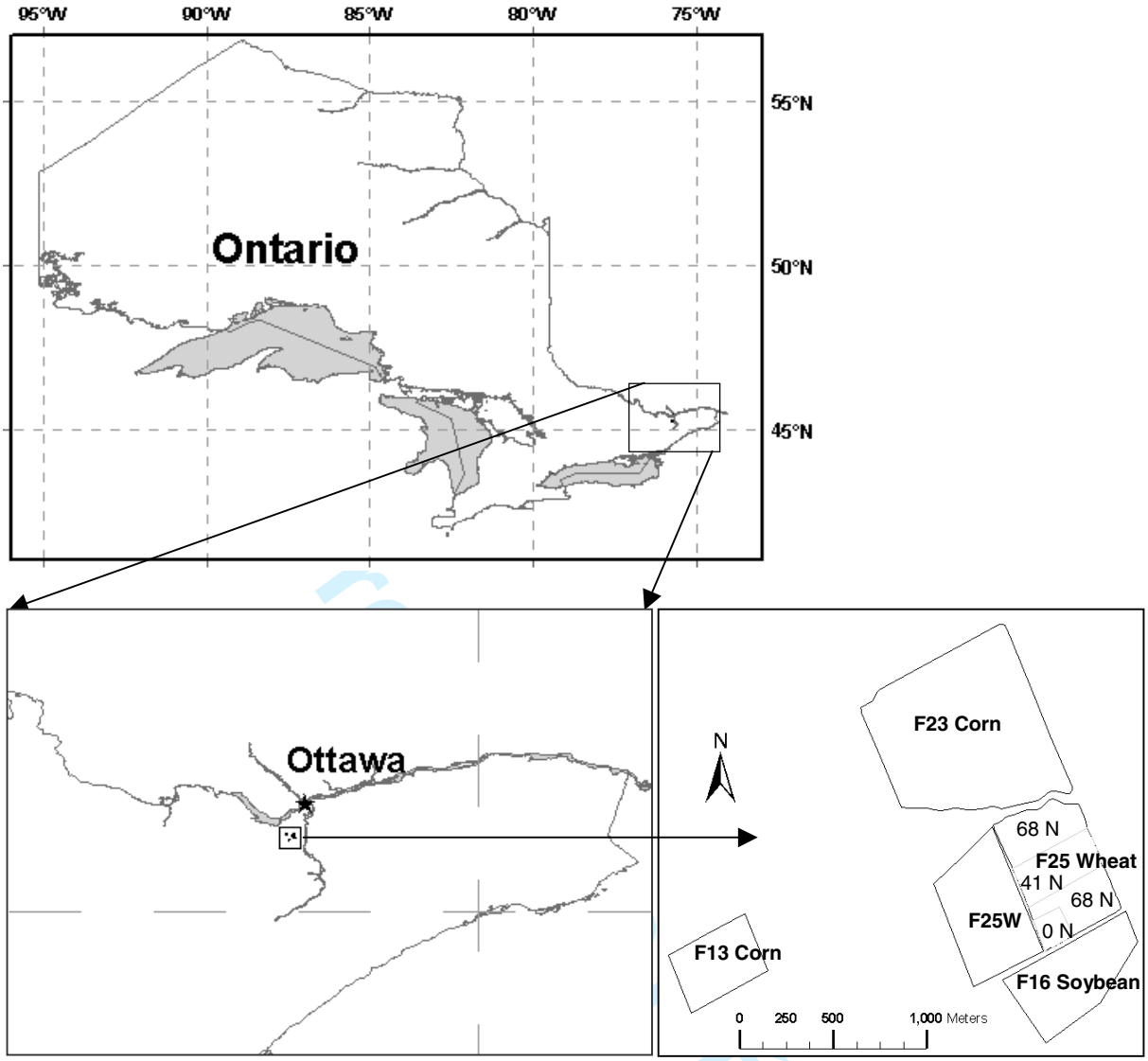

Figure 2

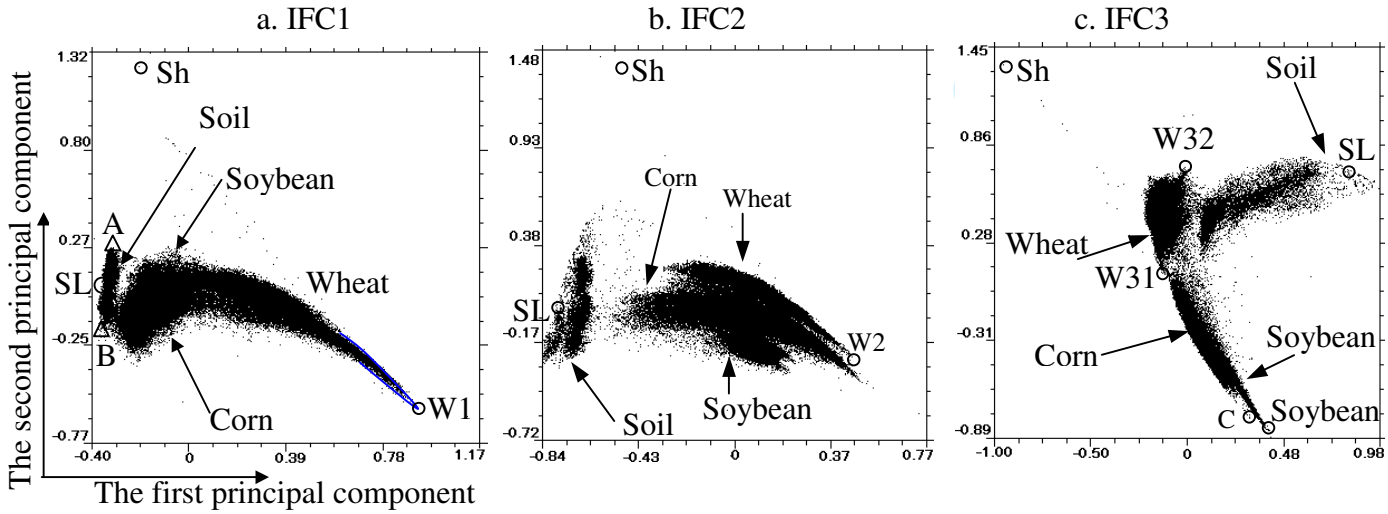

Figure 3

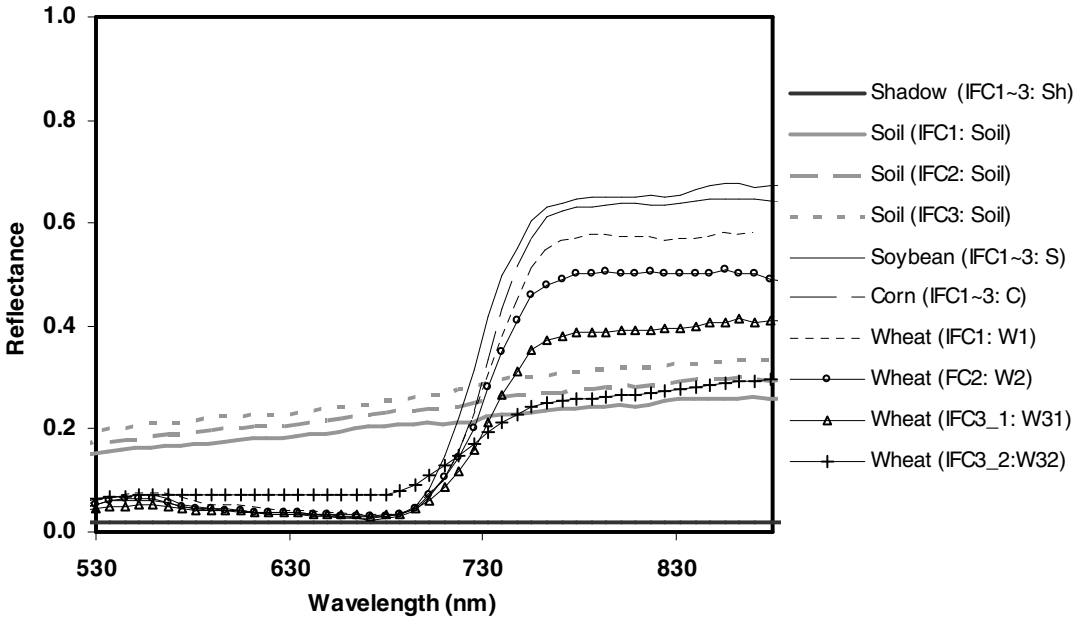

Figure 4

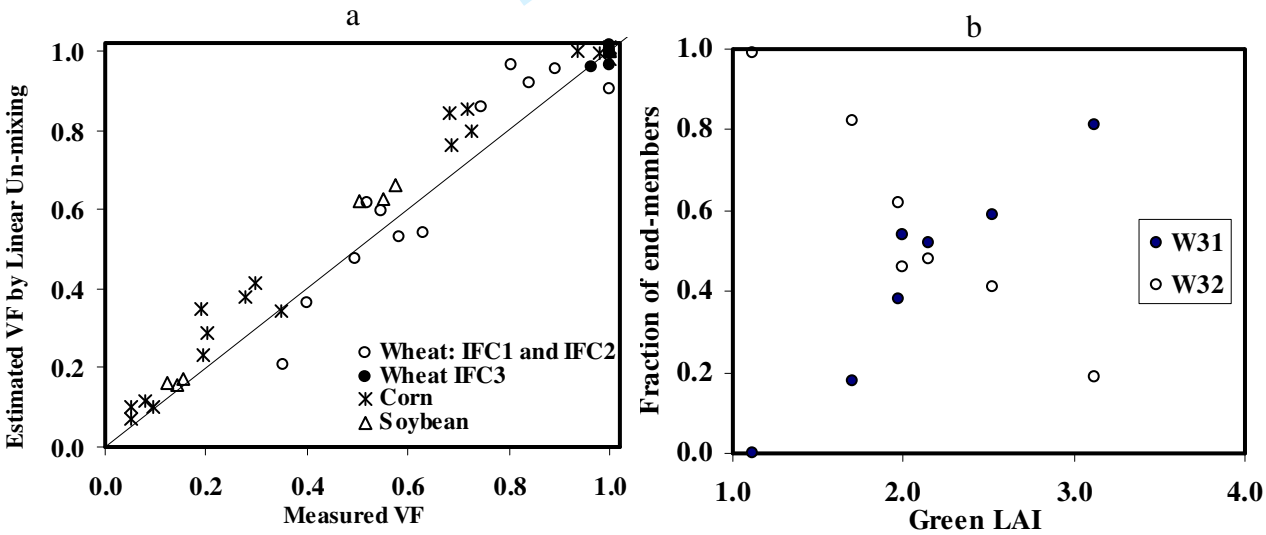

Figure 5

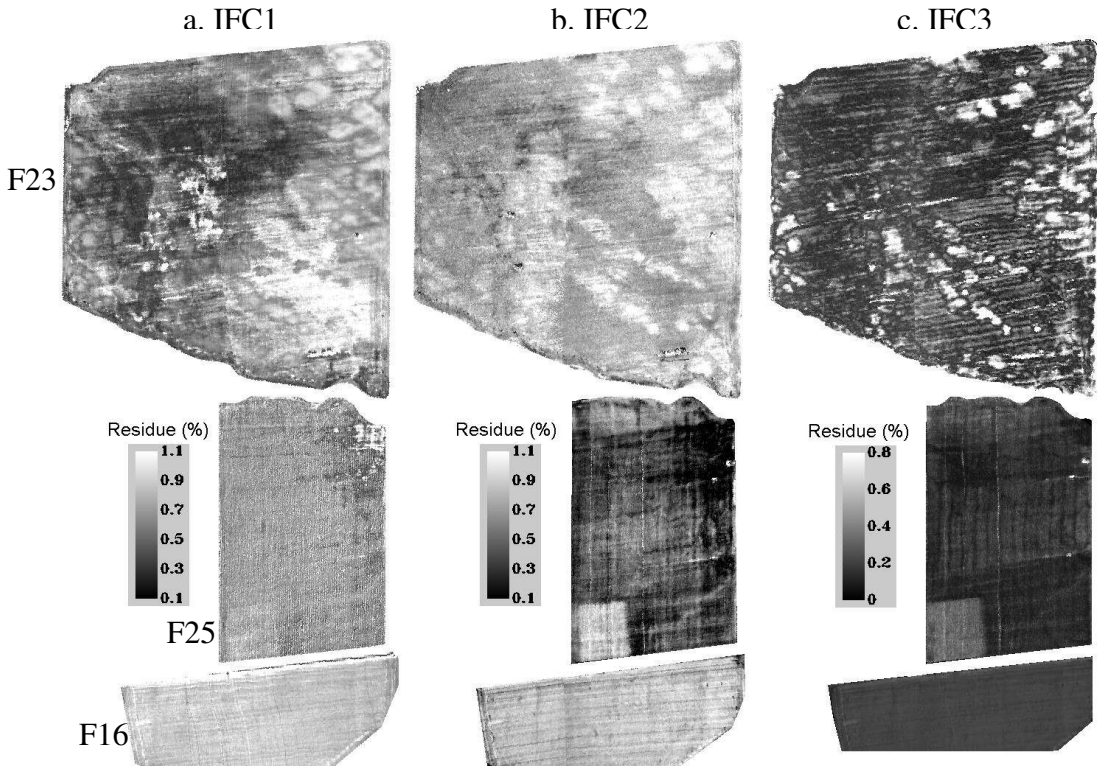

Figure 6

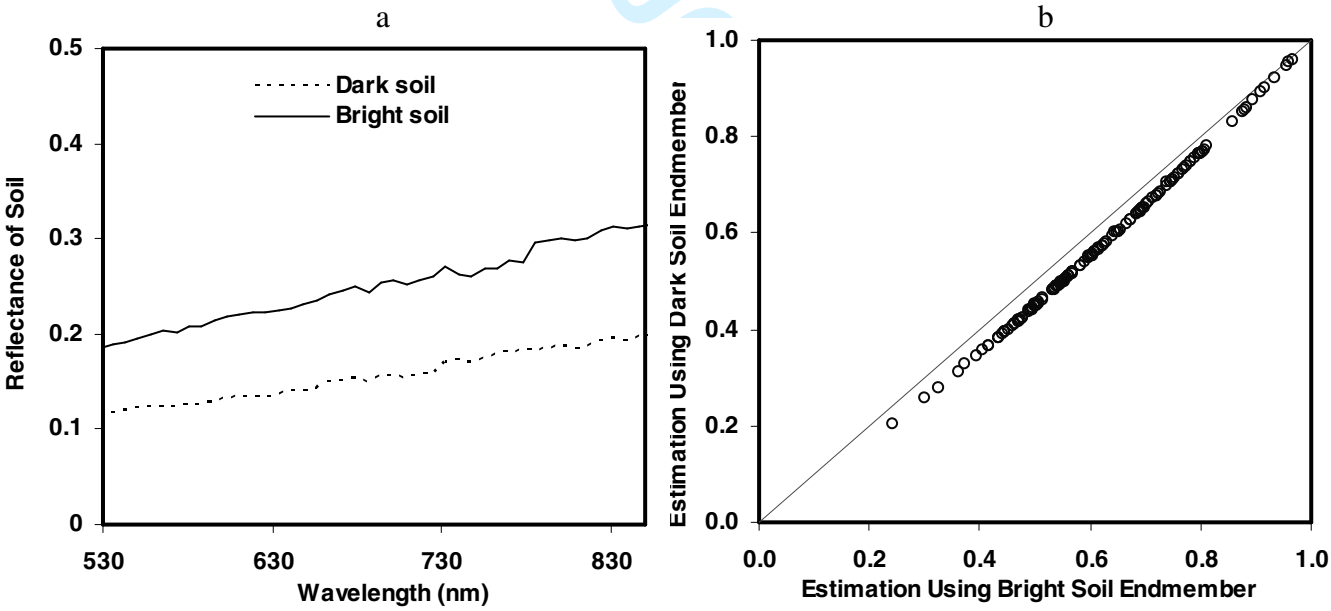

Figure 7

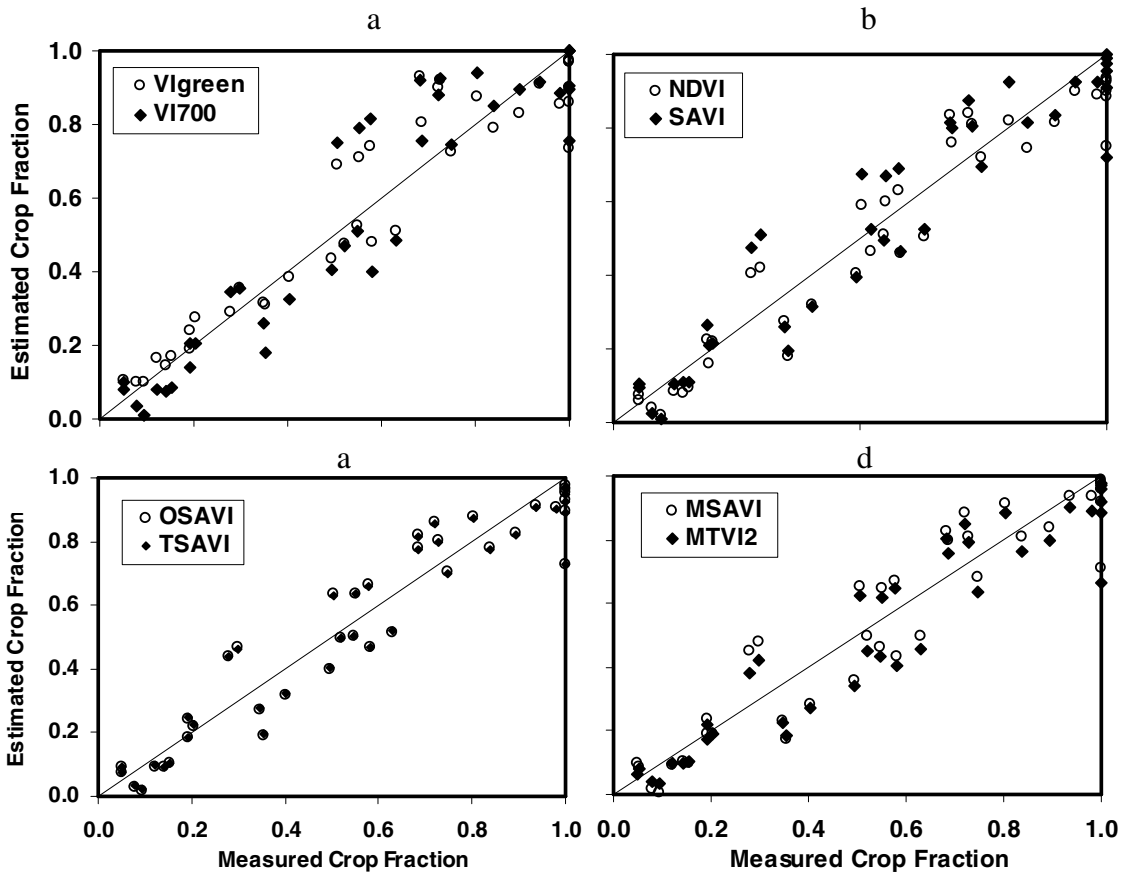

Figure 8

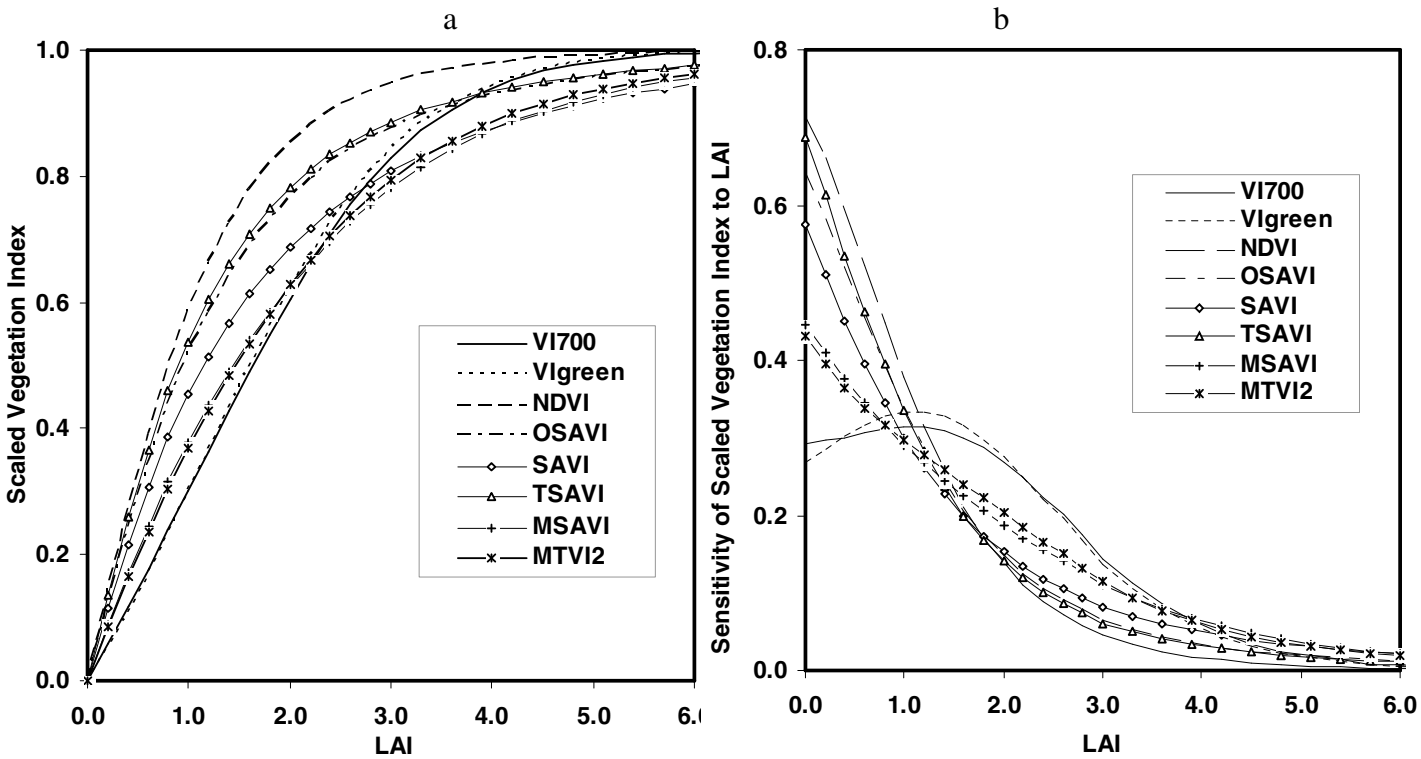

Figure 9

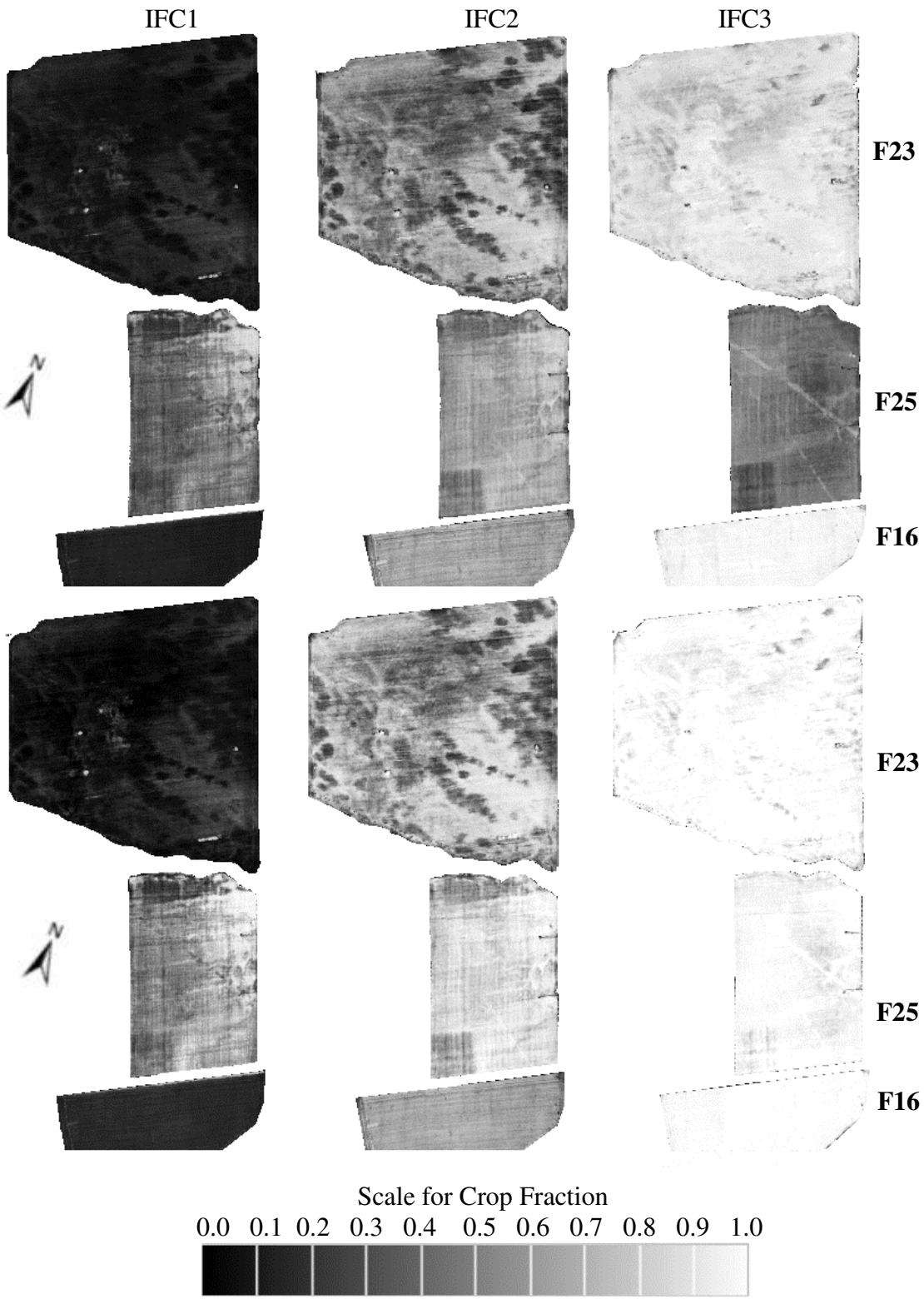
IFC1
IFC2
IFC3
F23
F25
F16
F23
F25
F16
N
N
Scale for Crop Fraction
0.0 0.1 0.2 0.3 0.4 0.5 0.6 0.7 0.8 0.9 1.0